ISSN 0036-0295, Russian Metallurgy (Metally), Vol. 2022, No. 10, pp. 1090–1095. © Pleiades Publishing, Ltd., 2022.
Russian Text © The Author(s), 2022, published in Deformatsiya i Razrushenie Materialov, 2022, No. 8, pp. 2–8.

PHYSICAL FOUNDATIONS OF STRENGTH AND PLASTICITY

Simulation of the Structural Changes in the Surface Layer of a Deformed BCC Crystal during a Short-Term External High-Intense Action

A. V. Markidonov[a, b], A. N. Gostevskaya[a, *], V. E. Gromov[a], M. D. Starostenkov[c], and P. A. Zykov[d]

[a] *Siberian State Industrial University, Novokuznetsk, 654007 Russia*

[b] *Kuzbas Humanitarian-Pedagogical Institute, Kemerovo State University, Novokuznetsk, 654027 Russia*

[c] *Polzunov Altai State Technical University, Barnaul, 656038 Russia*

[d] *Branch of Gorbachev Kusbas State Technical University, Novokuznetsk, 654005 Russia*

**e-mail: lokon1296@mail.ru*

Received April 20, 2022; revised April 20, 2022; accepted April 27, 2022

Abstract—Molecular dynamics simulation of the changes in a α-Fe surface layer during short-time high-energy action is performed. The developed model enables us to reveal the continuity violation of the surface layer, which consists in excess free volume localization in the form of spherical pores. The sizes of these imperfections and the duration of their existence are substantially dependent on the radiation energy density and the deformation of a calculation cell.

Keywords: laser ablation, molecular dynamics simulation, pulsed treatment, bcc-crystal, pore, surface, deformation

DOI: 10.1134/S0036029522100305

INTRODUCTION

The irradiation of a metal with ultra-short superpower laser pulses creates unique physical conditions, such as a high material heating rate and a volumetric mechanism of releasing laser radiation energy. As a result, a condensed medium is heated to temperatures higher than the equilibrium melting and vaporization temperatures. The time of action of picoseconds laser pulses is comparable with characteristic times of thermalization and phase transformations in a material, but, in this case, the thermal effect behind the treatment zone is minimal. Doubtlessly, the processes of nonequilibrium heating of a substance during laser irradiation are of a practical interest and, thus, they are objects of various experimental and theoretical studies [1–4].

Irradiation with high-power laser pulses can lead to substance melting and melt motion caused by sharp temperature gradients and the relaxation of pressure with subsequent separation (ablation) of a substance from its surface, which is used in various areas [5–9]. The rate of these processes can be so high that it does not allow direct studies of them. In this case, it is most rational to use computer simulation methods, which allows a consideration of complex systems due to the increasing computational power of modern computers. Laser ablation has been successfully studied by molecular dynamics method [10–12], although a number of assumption is used [13, 14]. Therefore, for example, it is necessary to consider, in terms of the classical molecular dynamics, the time intervals corresponding to the characteristic electron–phonon relaxation time.

The structural changes occurring in an amorphous phase at the stage of cool-down after the end of irradiation undoubtedly influence the physical and geometrical characteristics of a completely or partially crystallized structure and, as a result, the formation of the material surface. Taking into account the abovementioned, the study of the amorphous structure of a material subjected to laser irradiation is of practical interest. In this work, the structural changes taking place in a material during high-temperature irradiation are studied by molecular dynamics simulation.

MODEL

The model was constructed as follows. In a rectangular coordinate system, the calculation cell sizes were set in three mutually orthogonal crystallographic directions coinciding with the coordinate axes. Then, a unit cell was formed: the arrangement of atoms in it corresponded to bcc lattice with an equilibrium parameter a_0 and all the prescribed volume was filled with such cells via translation. The calculation cell was a rectangular parallelepiped with a side ratio of 3 : 4 : 25

containing 48000 atoms. Since we assumed to conduct studies on an iron crystallite model, the lattice parameter was taken to be 2.866 Å.

Along axes X and Z, periodic boundary conditions were used; along axis Y, free boundary conditions imitating the crystal surface were used. The calculation cell was oriented in the space so that axis X coincided with crystallographic direction [100], axis Y, with direction [010], and axis Z, with direction [001].

A potential constructed using the embedded-atom method was used as a function of the interparticle interaction [15]. The equations of motion describing the behavior of a system of particles were integrated using the velocity Verlet algorithm at a time step of 1 fs. The calculations were carried out with the XMD software package [16]. The visualization of the simulation results was performed using the OVITO visualization package [17].

To simulate the heating of the target under laser radiation, the calculation cell was divided into 10 layers of the same thicknesses along axis Y, in each of which we prescribed a certain temperature decreasing with the distance from the surface. As there is heat equilibrium between electrons and phonons, heat propagation can be described by a heat conduction model. For a half-infinite solid body, an analytical exact solution to a thermal problem can be obtained by integral transformations [18]. In this case, if the source intensity is independent of time and the physical parameters are constant and independent of temperature (linear thermal conduction problem), the temperature distribution over the sample thickness at the heating stage (at $t < \tau$, where τ is the irradiation time) is determined as a function of coordinates as follows:

$$T(y,t) = \frac{2Aq}{\lambda}\sqrt{\alpha t}\, ierfc\left(\frac{y}{2\sqrt{\alpha t}}\right), \quad (1)$$

where A is the absorption capacity, q is the energy density, λ is the thermal conductivity, and α is the thermal diffusivity.

Function $ierfc(x)$ entering into Eq. (1) is the integral of an additional probability integral,

$$ierfc(x) = \int_x^\infty ierfc(x)dx. \quad (2)$$

After the end of laser irradiation ($t > \tau$), a cooling stage takes place, and the temperature distribution is determined as follows:

$$T(y,t) = \frac{2Aq}{\lambda} \times \left[\sqrt{\alpha t}\, ierfc\left(\frac{y}{2\sqrt{\alpha t}}\right) - ierfc\left(\frac{y}{2\sqrt{\alpha(t-\tau)}}\right)\right]. \quad (3)$$

The temperature was calculated using the following values of the parameters corresponding to the simulated material and picosecond laser pulses: $A = 0.68$, $q = 3.0$–6.5 MW/cm^2, $\lambda = 80$ W/(m K), $\alpha = 2.621 \times 10^{-5}$ m^2/s, $\tau = 10 \times 10^{-12}$ s.

Nonuniform heating of the simulated sample can lead to the formation, near the surface, of a compression region propagating to the depth in the form of a pressure wave; as it reaches the opposite boundary in the case of free boundary conditions, it can favor atom ejection. To avoid it, the temperature in the layer farthest from the simulated surface was maintained at 300 K using a thermostating procedure; in addition, viscous boundary conditions were imposed.

The simulation process consisted of two stages. At the initial stage, the calculation cell was subjected to nonuniform heating in 10 ps of the simulation time according to Eq. (1). Then, during the second stage, the calculation cell was cooled in 20 ps, and its temperature was established according to Eq. (3).

The structural changes in the near-surface layers of the calculation cell were quantitatively estimated using porosity coefficient θ determined as the fraction of the free surface formed by voids to the total free surface identified in a calculation cell.

Biaxial crystal deformation was induced by a change in the interatomic distance in the calculation cell along axes X and Z.

RESULTS AND DISCUSSION

Figure 1 shows the theoretical curves of the temperature distribution along axis Y calculated by Eq. (1) and the averaged temperatures of the selected layer of the calculation cell at a laser radiation energy density q =3.5 MW/cm^2. According to these data, the temperature of the layer farthest from the surface does not correspond to the calculated values, which is due to the application of the thermostating procedure. Taking this fact into account, we do not consider the structure of the lower layer in this work. Figure 2 shows the change in the average temperature of the calculation cell during the simulation.

After the local temperature of the calculation cell at the heating stage becomes higher than the melting temperature, a phase transition occurs and the interface between the solid and liquid phases shifting to the region of lower temperatures forms in the cell. The successive increase in the temperature leads to the fact that atoms start to be detached (evaporated) from the surface of the calculation cell, forming a cloud. The cooling stage is accompanied by the localization of the low-density regions formed at the previous heating stage (Fig. 3a), their coalescence, and the formation of spherical pores (Figs. 3b–3d). Note that the formation of nanopores in the surface layer during laser irradiation was also observed in [19].

To identify the voids and to estimate their surface area, we used the algorithm [20] based on the Edelsbrunner and Mücke alpha-form method, in which a geometric set of points is jointed by a surface mesh

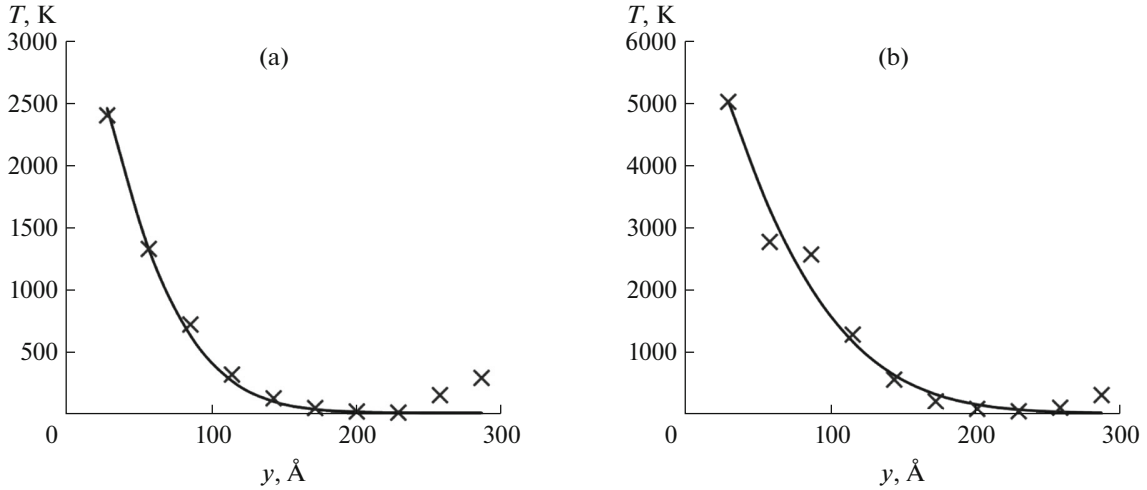

Fig. 1. (Solid line) Calculated change in the temperature vs. the distance from the crystal surface and (markers) averaged temperature of the selected layers of the calculation cell after (a) 1 and (b) 12 ps of model time (q = 3.5 MW/cm^2).

using the Delaunay tetrahedrization with the subsequent smoothing procedure. The identification of the void in the solid body volume is determined by the radius of a virtual sphere that fits into interatomic spaces. The radius of such a sphere should be at least larger than half the shortest interatomic distance; alternatively, "artificial" voids are included into the calculations. In this work, the virtual sphere radius is taken to be the lattice parameter.

When simulating various densities of the absorbed radiation energy reached by varying parameter q in Eqs. (1) and (3), we observe various structural changes in the near-surface layers of the calculation cell. For example, at $q \le 3.5$ MW/cm^2, the voids formed in the cell are dissolved during simulation (Fig. 4). At larger q, we observe the formation of extended voids, which are stable during the entire simulation, in a amorphous region (such defects are the objects of future studies).

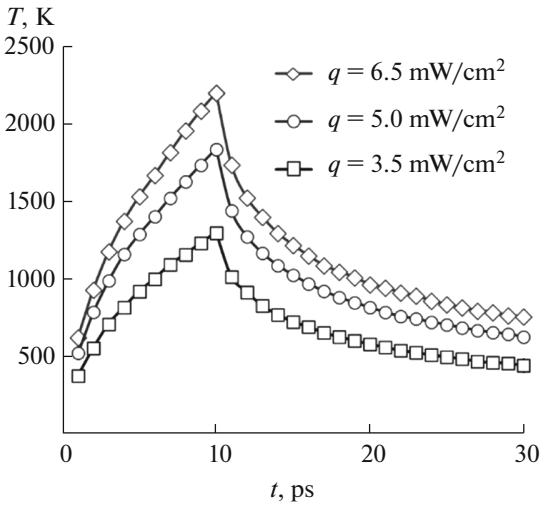

Fig. 2. Time dependences of the average calculation cell temperature at various laser radiation energy densities.

The mechanism of dissolution of pores in the surface layer of the calculation cell is a diffusion-viscous flow of the material into the void formed. The diffusion process rate is mainly determined by temperature and, therefore, the pore stability at the second simulation stage will be dependent on the cooling rate of the calculation cell. This value is estimated at 3.53×10^{13} K/s for cooling according to Eq. (3). To reach other rates, we added coefficient $(\tau/t)n$ in Eq. (3) (where n is an arbitrary rational number). By varying n, we obtained higher cooling rates, at which the porosity of the upper layer is retained. Figure 5 shows the simulation results.

As concentrated energy sources act on a material locally, high-gradient temperature fields leading to the development of various deformation appear inevitably [21, 22]. In this connection, it is interesting to study the evolution of the pores having formed in the surface layer of a crystal subjected to deformation. For the porosity coefficient to characterize pore development more clearly, we cut off small void sizes by doubling the radius of the virtual sphere used for their identification.

Figure 6 shows the results of calculation at various strains. From these data, it follows that tensile deformation favors the formation of coarser pores in the surface layer and also stabilizes them; as a result, pores are retained for a longer time as compared to the pores in the undeformed crystal. Conversely, compression of the calculation cell favors fast dissolution of pores, and a further increase in the strain prevents their formation.

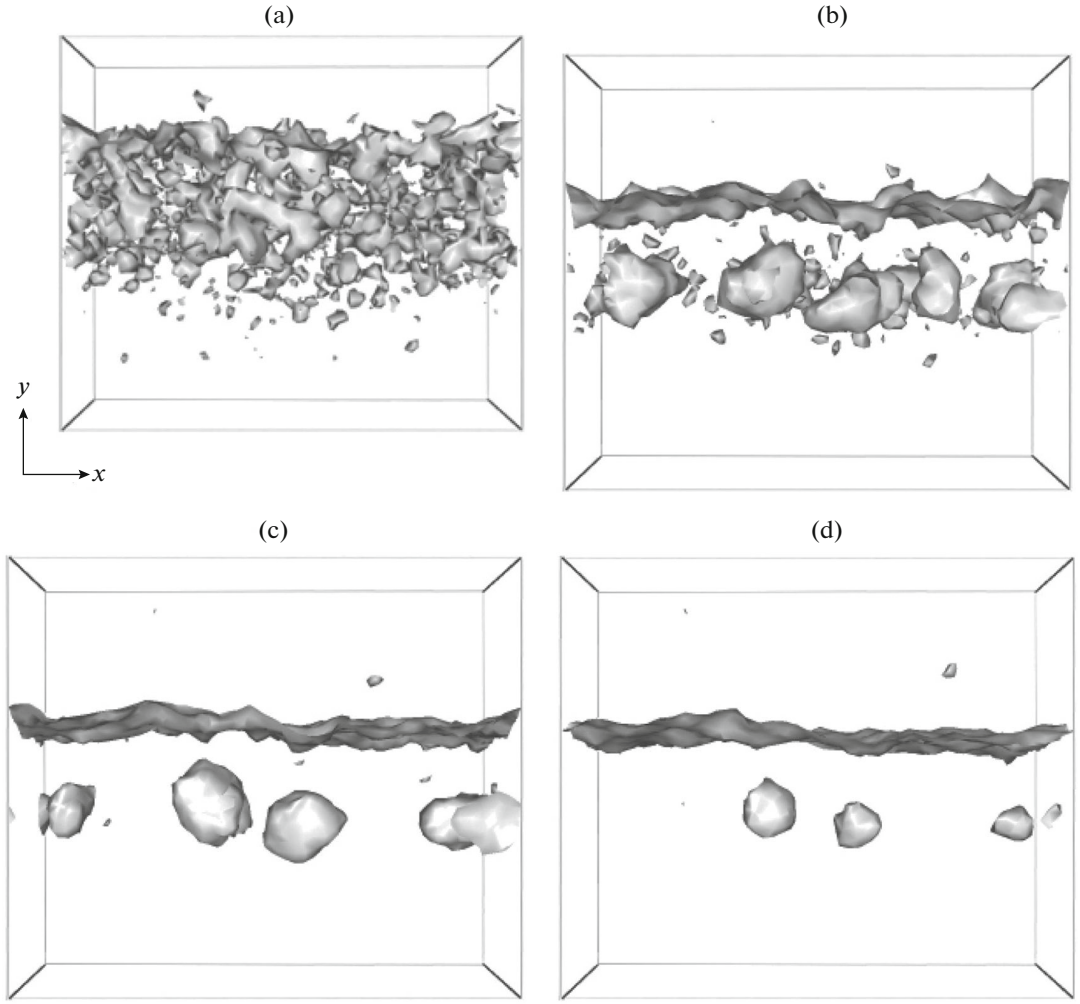

Fig. 3. Visualization of the free surface having formed in a calculation cell (its fragment is shown) after (a) 11, (b) 15, (c) 19, and (d) 22 ps of model time (q = 3.5 MW/cm^2).

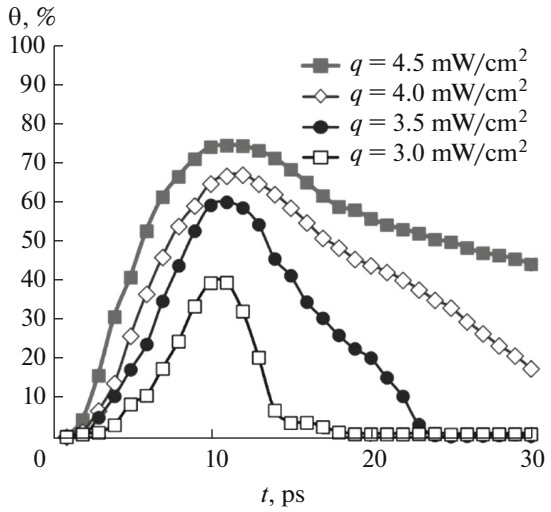

Fig. 4. Time dependences of the porosity coefficient of a calculation cell at various laser radiation energy densities.

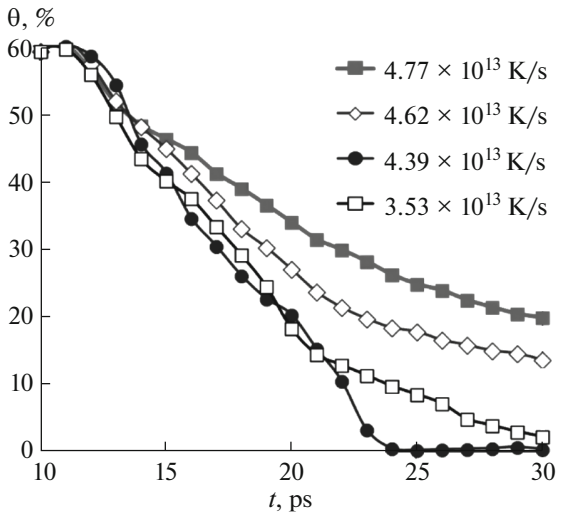

Fig. 5. Time dependences of the porosity coefficient of a calculation cell at the finishing simulation stage and various cooling rates (q = 3.5 MW/cm^2).

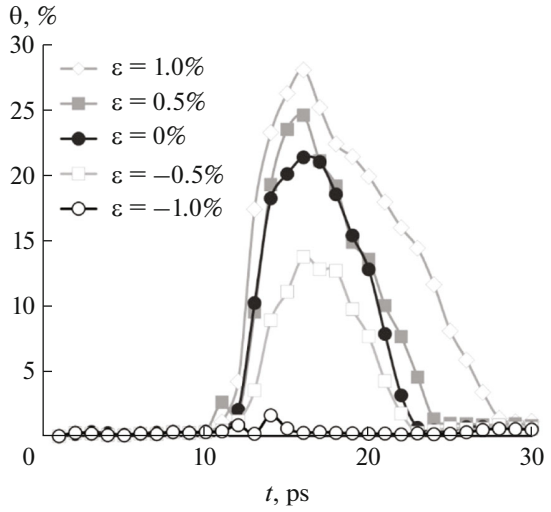

Fig. 6. Time dependences of the porosity coefficient of a calculation cell at various strains (q = 3.5 MW/cm^2).

CONCLUSIONS

An external high-energy action on the solid body surface, for example, by ultrashort superpower laser pulses, can lead to phase transitions, the results of which are radical changes in the surface structure. The similar fast processes in solids are successfully studied by computer simulation methods. In this work, we constructed a molecular dynamics simulation for studying the processes proceeding in the surface layers of a material under external short-time high-energy irradiation. After the end of an external action, the free volume in the surface layer was found to be localized as a group of pores, which dissolve during shrinkage. These pores can be stabilized by increasing the cooling rate of a calculation cell or by creating tensile deformation. On the other hand, compression of the calculation cell allows one to exclude pore formation completely. The results of this study can be used for studying the processes of laser ablation and surface modification.

FUNDING

This work was supported by the Ministry of Higher Education and Science of the Russian Federation, project no. 0809-2021-0013.

CONFLICT OF INTEREST

The authors declare that they have no conflicts of interest.

REFERENCES

1. A. A. Ionin, S. I. Kudryashov, and A. A. Samokhin, "Ablation of material surfaces under action of ultrashort laser pulses," Usp. Fiz. Nauk **187** (2), 159–172 (2017).
2. A. V. Starinskiy, Y. G. Shukhoy, and A. V. Bulgakov, "Laser-induced damage thresholds of gold, silver, and their alloys in air and water," Appl. Surf. Sci. **396**, 1765–1774 (2017).
3. Y. V. Petrov, V. A. Khokhlov, V. V. Zhakhovsky, and N. A. Inoganov, "Hydrodynamic phenomena induced by laser ablation of metal into liquid," Appl. Surf. Sci. **492**, 285–297 (2019).
4. B. Rajcic, S. Petronic, K. Colic, Z. Stevic, A. Petrovic, Ž. Mišcovic, and D. Milovanovic, "Laser processing of Ni-based superalloy surface susceptible to stress concentration," Metals **11**, 750 (2021).
5. N. A. Smirnov, S. I. Kudryashov, P. A. Danilov, A. A. Rudenko, B. Gakovic, D. Milovanović, A. A. Ionin, A. A. Nastulyavichus, and S. F. Umanskaya, "Microprocessing of a steel surface by single pulses of variable width," Laser Phys. Lett. **16** (5), 056002 (2019).
6. C. Y. Shih, C. Wu, M. V. Shugaev, and L. V. Zhigilei, "Atomistic modeling of nanoparticle generation in short pulse laser ablation of thin metallic films in water," J. Colloid and Interf. Sci. **489**, 3–17 (2017).
7. P. A. Danilov, A. A. Ionin, S. I. Kudryashov, A. A. Rudenko, I. N. Saraeva, and D. A. Zayarny, "Non-monotonic variation of Au nanoparticle yield during femtosecond/picoseconds laser ablation in water," Laser Phys. Lett. **14** (5), 056001 (2017).
8. E. L. Gurevich, Y. Levy, S. V. Gurevich, and N. M. Bulgakova, "Role of the temperature dynamics in formation of nanopatterns upon single femtosecond laser pulses on gold," Phys. Rev. **95** (5), 054305 (2017).
9. A. Ionin, A. Ivanova, R. Khmel'nitskii, Y. Klevkov, S. Kudryashov, N. Mel'nik, A. Nastulyavichus, A. Rudenko, I. Saraeva, and D. Zayarny, "Milligram-per-second femtosecond laser production of Se nanoparticle inks and ink-jet printing of nanophotonic 2D-patterns," Appl. Surf. Sci. **436**, 662–669 (2018).
10. J.-K. Kuo, P.-H. Huang, S.-K. Chien, K.-Y. Huang, and K.-T. Chen, "Molecular dynamics simulation of crater formation induced by laser ablation on the surface of α-Fe substrate," MATEC Web of Conf. **167**, 03011 (2018).
11. D. S. Ivanov, A. Blumenstein, P. Simon, M. E. Garsia, and B. Rethfeld, "Molecular dynamics modeling of periodic nanostructuring of metals with a short UV laser pulse under spatial confinement by a water layer," Appl. Phys. A. **123** (12), 744 (2017).
12. Q. S. Bai, Y. H. Li, R. Q. Shen, K. Zhang, X. X. Miao, and F. H. Zhang, "Molecular simulation and ablation property on thelaser-induced metal surface," in *Proceedings of Pacific Rim Laser Damage 2019 Conference. Optical Materials for High-Power Lasers* (Qingdao, 2019), Vol. 11063, 1106306.
13. A. N. Gostevskaya, "Action of ultrashort superpower laser pulses on a solid," in *Proceedings of XXVI Ural School of Metallurgist–Heat Treater Conference on Challenging Problems of the Physical Metallurgy of Steels and Alloys* (Ural Univer., Yekaterinburg, 2022), pp. 259–261.
14. A. N. Gostevskaya, A. V. Markidonov, and V. V. Kovalenko, "Molecular-dynamics simulation of laser ablation," in *Proceedings of International Symposium on*

Promising Materials and Technologies (BelGISS, Minsk, 2021), pp. 21–22.

15. M. I. Mendelev, S. Han, D. J. Srolovitz, G. J. Ackland, D. Y. Sun, and M. Asta, "Development of new interatomic potentials appropriate for crystalline and liquid iron," Phil. Mag. **83** (35), 3977–3994 (2003).
16. XMD—Molecular Dynamics for Metals and Ceramics, http://xmd.sourceforge.net/about.html. Cited April 15, 2022.
17. A. Stukowski, "Visualization and analysis of atomistic simulation data with OVITO—the Open Visualization Tool," Modeling and Simulation Mater. Sci. Eng. **18**, 015012 (2010).
18. N. P. Rykalkin, A. A. Uglov, I. V. Zuev, and A. N. Kokora, *Laser and Electron-Beam Treatment of Materials: A Handbook* (Mashinostroenie, Moscow, 1985).
19. S. P. Murzin, A. V. Prokofiev, and A. I. Safin, "Study of Cu–Zn alloy objects vibration characteristics during laser-induced nanopores formation," Procedia Eng. **176**, 552–556 (2017).
20. A. Stukowski, "Computational analysis methods in atomistic modeling of crystals," J. Min., Met. & Mater. Soc. **662** (3), 399–407 (2014).
21. T. V. Malinskii, V. E. Rogalin, and V. A. Yamshchikov, "Plastic deformation of copper and its alloys under the action of nanosecond UV laser pulse," Phys. Met. Metallogr. **123**, 178–185 (2022).
22. F. Yin, X. Ye, H. Yao, P. Wei, X. Wang, J. Cong, and Y. Tong, "Surface forming criteria of Ti–6Al–4V titanium alloy under laser loading," Appl. Sci. **11**, 5406 (2021).

Translated by Yu. Ryzhkov